

Electronic Supplementary Information for:
Towards focusing of a swarm of magnetic micro/nanomotors

Konstantin I. Morozov^{1*} and Alexander M. Leshansky^{1,2}

¹*Department of Chemical Engineering,*

²*Russel Berrie Nanotechnology Institute (RBNI)*

Technion – Israel Institute of Technology, Haifa 32000, Israel

(Dated: July 7, 2020)

* mrk@technion.ac.il

I. Rotation matrix

We use the definition of the three Euler angles φ , θ and ψ following Ref. [1]. The components of any vector \mathbf{W} in the body-fixed coordinate system (BCS) and in the laboratory coordinate system (LCS) are determined from the relation $\mathbf{W}^{BCS} = \mathbf{R} \cdot \mathbf{W}$, where \mathbf{R} is the rotation matrix. The rotation matrix is expressed explicitly via the Euler angles [2]

$$\mathbf{R} = \begin{pmatrix} c_\varphi c_\psi - s_\varphi s_\psi c_\theta & s_\varphi c_\psi + c_\varphi s_\psi c_\theta & s_\psi s_\theta \\ -c_\varphi s_\psi - s_\varphi c_\psi c_\theta & -s_\varphi s_\psi + c_\varphi c_\psi c_\theta & c_\psi s_\theta \\ s_\varphi s_\theta & -c_\varphi s_\theta & c_\theta \end{pmatrix},$$

where we use the compact notation, $s_\psi = \sin \psi$, $c_\theta = \cos \theta$, etc.

II. Planar symmetric V-shape propeller

As an example, we consider the V-shape propeller with 120° central angle with the arm width-to-height aspect ratio $w : h = 2 : 1$. It is shown in Figs. S1a,b along with the principal

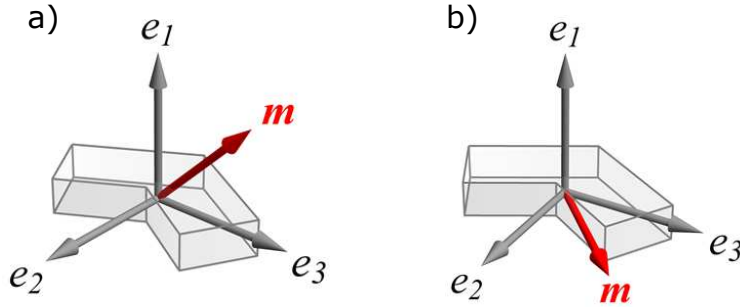


FIG. S1. The symmetric planar V-shape propeller has a central angle of 120° , the cross-section aspect ratio 2:1 and it is magnetized a) off-plane ($\Phi = \pi/4$, $\alpha = 0$) and b) in-plane ($\Phi = \pi/4$, $\alpha = \pi/2$).

axes of rotation $\{\mathbf{e}_1, \mathbf{e}_2, \mathbf{e}_3\}$ (i.e., the eigenvectors of \mathcal{F}). Magnetization orientation plays a key role in propulsion. We consider the cases of off-plane and in-plane magnetization (see Fig. S1). For the former, there are two magnetization components – along the easy axis \mathbf{e}_3 of the body rotation and along the normal vector to the plane of the object, as shown in Fig. S1a. For the latter, both magnetization components belong to the plane of the V-structure (see Fig. S1b).

Using the multipole expansion algorithm [3] we determine the coupling and rotational mobilities of the planar propeller

$$\mathcal{G}^{\text{V-shape}} = \frac{10^{-2}}{\eta\ell^2} \begin{pmatrix} 0 & 0 & -1.058 \\ 0 & 0 & 0 \\ -1.058 & 0 & 0 \end{pmatrix}, \quad \mathcal{F}^{\text{V-shape}} = \frac{1}{\eta\ell^3} \begin{pmatrix} 1.067 & 0 & 0 \\ 0 & 1.078 & 0 \\ 0 & 0 & 2.945 \end{pmatrix}, \quad (\text{S1})$$

where η stands for the dynamics viscosity and $\ell = 2.732h$ for the propeller's length, with h being the V-shape thickness. The transverse rotational friction anisotropy parameter is negligibly small, $\varepsilon = (\mathcal{F}_2 - \mathcal{F}_1)/(\mathcal{F}_2 + \mathcal{F}_1) = 0.004$. The longitudinal rotational anisotropy parameter is $p = \mathcal{F}_3/\mathcal{F}_\perp = \frac{1}{2}\mathcal{F}_3(\mathcal{F}_1^{-1} + \mathcal{F}_2^{-1}) = 2.743$. The only non-trivial coupling coefficients are $\mathcal{G}_{13} = \mathcal{G}_{31} = -0.01058/(\eta\ell^2)$.

The *chirality matrix* \mathbf{Ch} with components $\text{Ch}_{ij} = \frac{1}{2\ell}\mathcal{G}_{ij}(\mathcal{F}_i^{-1} + \mathcal{F}_j^{-1})$ (no summation over the repeating indices) [4] have the form

$$\mathbf{Ch}^{\text{V-shape}} = 10^{-2} \begin{pmatrix} 0 & 0 & -0.675 \\ 0 & 0 & 0 \\ -0.675 & 0 & 0 \end{pmatrix}. \quad (\text{S2})$$

Average velocity of the symmetric V-shape propeller

In the laboratory frame the propulsion velocity of the driven object reads

$$\mathbf{U} = \mathbf{R}^+ \cdot \mathcal{G} \cdot \mathcal{F}^{-1} \cdot \boldsymbol{\Omega}, \quad (\text{S3})$$

where \mathbf{R}^+ is the transposed rotation matrix, \mathcal{G} and \mathcal{F} are the coupling and rotation \mathcal{F} viscous mobility tensors and $\boldsymbol{\Omega}$ is its angular velocity. For planar symmetric V-shaped propeller the only nontrivial elements of the coupling matrix are $\mathcal{G}_{13} = \mathcal{G}_{31}$ (see Eq. (S1)).

Then the velocity components (S3) take the form:

$$\frac{U_X}{\mathcal{G}_{13}} = [s_\varphi s_\psi (s_\theta^2 \mathcal{F}_1^{-1} - c_\theta^2 \mathcal{F}_3^{-1}) + c_\varphi c_\psi \mathcal{F}_3^{-1}] \dot{\varphi} + (c_\varphi c_\psi - s_\varphi s_\psi c_\theta) \mathcal{F}_3^{-1} \dot{\psi} + s_\varphi c_\psi s_\theta \mathcal{F}_1^{-1} \dot{\theta}, \quad (\text{S4})$$

$$\frac{U_Y}{\mathcal{G}_{13}} = [c_\varphi s_\psi (c_\theta^2 \mathcal{F}_3^{-1} - s_\theta^2 \mathcal{F}_1^{-1}) + s_\varphi c_\psi \mathcal{F}_3^{-1}] \dot{\varphi} + (s_\varphi c_\psi + c_\varphi s_\psi c_\theta) \mathcal{F}_3^{-1} \dot{\psi} - c_\varphi c_\psi s_\theta \mathcal{F}_1^{-1} \dot{\theta}, \quad (\text{S5})$$

$$\frac{U_Z}{\mathcal{G}_{13}} = s_\psi s_\theta c_\theta (\mathcal{F}_1^{-1} + \mathcal{F}_3^{-1}) \dot{\varphi} + s_\psi s_\theta \mathcal{F}_3^{-1} \dot{\psi} + c_\psi c_\theta \mathcal{F}_1^{-1} \dot{\theta}. \quad (\text{S6})$$

In the tumbling and low-frequency wobbling regimes, the orientations are expressed as the asymptotic series in powers of the parameter δ (see Eqs. (11)-(13) in the main text):

$$\theta = \theta_0 + (Ac_{\omega t} + Bs_{\omega t})\delta + \theta_2\delta^2, \quad (\text{S7})$$

$$\varphi = \omega t + \varphi_0 + (Ec_{\omega t} + Fs_{\omega t})\delta + \varphi_2\delta^2, \quad (\text{S8})$$

$$\beta = \beta_0 + (Gc_{\omega t} + Hs_{\omega t})\delta + \beta_2\delta^2. \quad (\text{S9})$$

The Euler angle ψ entering the velocity equations (S4)-(S6) and the angle β in the orientation expansions (S7)-(S9) are related as $\beta = \psi + \alpha$, where α is the azimuthal angle of the propeller magnetic moment \mathbf{m} in the body frame: $\mathbf{m}^{\text{BCS}} = m(\sin \Phi \cos \alpha, \sin \Phi \sin \alpha, \cos \Phi)$. For $\alpha = 0$ and $0 < \Phi < \pi/2$ the V-shaped propeller is magnetized off-plane as shown in Fig. S1a, while for $\alpha = \pi/2$ and $0 < \Phi < \pi/2$ it is magnetized in-plane, see Fig. S1b. Here we consider an arbitrary value of the angle α .

In the tumbling regime, $\tilde{\omega} < \tilde{\omega}_{t-w}$, the coefficients in expansions (S7)-(S9) are (see Sec. III.A of the main text)

$$A = B = G = H = \theta_2 = \beta_2 = 0, \quad E = 2\tilde{\omega}\sqrt{1 - \tilde{\omega}^2}, \quad F = 2\tilde{\omega}^2 - 1, \quad \varphi_2 = -\frac{3}{4}\frac{\tilde{\omega}}{\sqrt{1 - \tilde{\omega}^2}}. \quad (\text{S10})$$

Substituting the expansions (S7)-(S9) into Eqs. (S4)-(S6) and averaging over the field period with the help of Eq. (S10) yields a zero value of the propulsion velocity \overline{U} .

In the low-frequency wobbling regime the coefficients in expansions (S7)-(S9) are given in Eqs. (17) of the main text:

$$\begin{aligned} A &= -2\tilde{\omega}(p-1) [\tilde{\omega}^2 + (p-1)c_{\Phi}^2] c_{\Phi}c_{\theta_0}/\Delta, \\ B &= \tilde{\omega}^2 p(p-1) s_{2\Phi} c_{\theta_0} c_{\beta_0}/\Delta, \\ E &= B\tilde{\omega}p/[(p-1)c_{\Phi}c_{\theta_0}], \\ F &= -1 - A\tilde{\omega}p/[(p-1)c_{\Phi}c_{\theta_0}], \\ G &= -B\tilde{\omega}/c_{\Phi}, \\ H &= A\tilde{\omega}/c_{\Phi}, \end{aligned} \quad (\text{S11})$$

where $\Delta = c_{\Phi}^4(p-1)^2 - c_{\Phi}^2\tilde{\omega}^2(p-1)^2 + \tilde{\omega}^2p^2$. Substitution of expansions (S7)-(S9) and (S11) into Eqs. (S4)-(S6) followed by averaging over the field period leads to the net translation

of the object with velocities:

$$\begin{aligned}
\bar{U}_X &= \delta B U_0, \quad \bar{U}_Y = -\delta A U_0, \\
U_0 &= \omega l \text{Ch}_{13} s_{2\bar{\theta}} s_{\bar{\beta}-\alpha}, \\
\bar{U}_Z &= U_0 + \omega l \text{Ch}_{13} (p-1) s_{2\bar{\theta}} \left(\frac{\Delta_4}{\Delta} s_{\bar{\beta}} c_\alpha - \frac{\Delta_5}{\Delta} c_{\bar{\beta}} s_\alpha \right) \delta^2,
\end{aligned} \tag{S12}$$

where

$$\Delta_4 = 2c_\Phi^4 (p-1) + c_\Phi^2 \tilde{\omega}^2 (p^2 + 1) - \tilde{\omega}^2 (p^2 + p\tilde{\omega}^2 - \tilde{\omega}^2), \tag{S13}$$

and

$$\Delta_5 = \Delta_4 - p^2 \tilde{\omega}^2 s_\Phi^2. \tag{S14}$$

The expressions (S12) determine the velocity of symmetric V-shape propeller in the low-frequency wobbling regime. For the particular cases of the off-plane and in-plane magnetization, depicted in Fig. S1a, and b, the expression in (S12) reduce to simpler equations (34)-(37) of the main text.

III. 2-turn helical propeller

Consider now the 2-turn magnetic helix with the 45° pitch angle, as shown in Fig. S2.

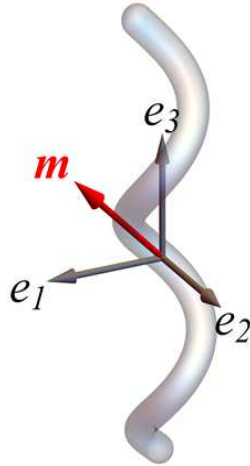


FIG. S2. The two-turn magnetic helix with the 45° pitch angle.

The viscous mobility coefficients of the helix were reported in [4]:

$$\mathcal{G}^{\text{helix}} = \frac{10^{-1}}{\eta l^2} \begin{pmatrix} 0 & 0 & 0.404 \\ 0 & -0.154 & 0 \\ 0.404 & 0 & 2.333 \end{pmatrix}, \quad \mathcal{F}^{\text{helix}} = \frac{1}{\eta l^3} \begin{pmatrix} 1.925 & 0 & 0 \\ 0 & 1.949 & 0 \\ 0 & 0 & 18.985 \end{pmatrix}. \quad (\text{S15})$$

The characteristic longitudinal swimmer size, $\ell = 30.8r$, where r is the radius of the filament cross-section. The longitudinal and transverse rotational friction anisotropy parameters are $p = 9.803$, $\varepsilon = 0.006$. The chirality matrix \mathbf{Ch} is given by

$$\mathbf{Ch}^{\text{helix}} = 10^{-2} \begin{pmatrix} 0 & 0 & 1.155 \\ 0 & -0.788 & 0 \\ 1.155 & 0 & 1.229 \end{pmatrix}. \quad (\text{S16})$$

Average velocity of the helix

In this section we consider the propulsion of a helix with arbitrary azimuthal angle α of magnetic moment and characterized by four nonzero coupling coefficients: \mathcal{G}_{22} , \mathcal{G}_{33} and $\mathcal{G}_{13} = \mathcal{G}_{31}$. Since \mathbf{U} in Eq. (S3) is proportional to \mathcal{G} , there are three contribution to the propulsion velocity of such a helix:

$$\mathbf{U}^{\text{helix}} = \mathbf{U}_1 + \mathbf{U}_2 + \mathbf{U}_3, \quad (\text{S17})$$

where $\mathbf{U}_1 \sim \mathcal{G}_{13}$, $\mathbf{U}_2 \sim \mathcal{G}_{22}$ and $\mathbf{U}_3 \sim \mathcal{G}_{33}$. The explicit relations for the components of \mathbf{U}_1 are given by Eqs. (S4)-(S6). The components of \mathbf{U}_2 and \mathbf{U}_3 follow from expression (S3) and they read:

$$\frac{U_{2,X}}{\mathcal{G}_{22}} = -(c_\varphi s_\psi + s_\varphi c_\psi c_\theta) \mathcal{F}_2^{-1}(c_\psi s_\theta \dot{\varphi} - s_\psi \dot{\theta}), \quad (\text{S18})$$

$$\frac{U_{2,Y}}{\mathcal{G}_{22}} = (-s_\varphi s_\psi + c_\varphi c_\psi c_\theta) \mathcal{F}_2^{-1}(c_\psi s_\theta \dot{\varphi} - s_\psi \dot{\theta}), \quad (\text{S19})$$

$$\frac{U_{2,Z}}{\mathcal{G}_{22}} = c_\psi s_\theta \mathcal{F}_2^{-1}(c_\psi s_\theta \dot{\varphi} - s_\psi \dot{\theta}), \quad (\text{S20})$$

$$\frac{U_{3,X}}{\mathcal{G}_{33}} = s_\varphi s_\theta \mathcal{F}_3^{-1}(c_\theta \dot{\varphi} + \dot{\psi}), \quad (\text{S21})$$

$$\frac{U_{3,Y}}{\mathcal{G}_{33}} = -c_\varphi s_\theta \mathcal{F}_3^{-1}(c_\theta \dot{\varphi} + \dot{\psi}), \quad (\text{S22})$$

$$\frac{U_{3,Z}}{\mathcal{G}_{33}} = c_\theta \mathcal{F}_3^{-1}(c_\theta \dot{\varphi} + \dot{\psi}), \quad (\text{S23})$$

The average value of the helix translation velocity equals to a sum of average contributions

$$\overline{\mathbf{U}}^{helix} = \overline{\mathbf{U}}_1 + \overline{\mathbf{U}}_2 + \overline{\mathbf{U}}_3, \quad (\text{S24})$$

Below we present the average velocity $\overline{\mathbf{U}}^{helix}$ of a helix in three regimes – tumbling, low-frequency wobbling and high-frequency wobbling.

A. Tumbling regime

In the tumbling regime, $\tilde{\omega} < \tilde{\omega}_{t-w}$, substituting the expansions (S7)-(S9) into Eqs. (S4)-(S6), (S18)-(S20), and (S21)-(S23) and averaging over the field period with the help of Eq. (S10) leads to

$$\overline{\mathbf{U}}_1 = \overline{\mathbf{U}}_3 = 0, \quad \overline{\mathbf{U}}_2 = \text{Ch}_2 c_\alpha^2 \omega \ell \mathbf{k}, \quad (\text{S25})$$

where \mathbf{k} is the unit vector along the Z -axis.

B. Low-frequency wobbling regime

In this case we substitute the expansions (S7)-(S9) into Eqs. (S4)-(S6), (S18)-(S20), and (S21)-(S23), but use the different relation (S11) for the coefficients. In this way we find:

$$\begin{aligned} \overline{U}_X &= \delta B U_0, \quad \overline{U}_Y = -\delta A U_0, \\ U_0 &= \omega \ell \left[\text{Ch}_{13} s_{2\bar{\theta}} s_{\bar{\beta}-\alpha} + \text{Ch}_2 s_{\bar{\theta}}^2 c_{\bar{\beta}-\alpha}^2 + \text{Ch}_3 c_{\bar{\theta}}^2 \right], \\ \frac{\overline{U}_Z}{\omega \ell} &= \frac{U_0}{\omega \ell} + \frac{\delta^2 (p-1)}{\Delta} \left[\text{Ch}_{13} s_{2\bar{\theta}} \left(\frac{\Delta_4}{\Delta} s_{\bar{\beta}} c_\alpha - \frac{\Delta_5}{\Delta} c_{\bar{\beta}} s_\alpha \right) + \right. \\ &\quad \left. + \text{Ch}_2 s_{\bar{\theta}}^2 \{ c_{\bar{\beta}}^2 \Delta_6 + s_{\bar{\beta}} c_{\bar{\beta}} s_{2\alpha} \Delta_8 + s_{\bar{\beta}}^2 s_\alpha^2 \Delta_9 \} + \text{Ch}_3 c_{\bar{\theta}}^2 \Delta_7 \right], \end{aligned} \quad (\text{S26})$$

where

$$\begin{aligned} \Delta_6 &= 2(p-1) (c_\Phi^4 - \tilde{\omega}^4), \\ \Delta_7 &= 2c_\Phi^2 [c_\Phi^2 (p-1) + \tilde{\omega}^2], \\ \Delta_8 &= \Delta_4 - \tilde{\omega}^2 [c_\Phi^2 + (p-1)\tilde{\omega}^2], \end{aligned} \quad (\text{S27})$$

$$\Delta_9 = -2[(p-1)(p^2-2)c_\Phi^4 + (p^3\tilde{\omega}^2 - p^3 - 2p^2\tilde{\omega}^2 + p^2)c_\Phi^2 - \tilde{\omega}^2(p^3 - 2p^2 - 2p\tilde{\omega}^2 + 2\tilde{\omega}^2)], \quad (\text{S28})$$

with the parameters Δ_4 and Δ_5 given earlier in Eqs. (S13) and (S14). The average values of $\bar{\theta}$ and $\bar{\beta}$ are reported in the main text (see Eqs. (19) and (20)):

$$\bar{\theta} = \arcsin \left[\frac{c_{\Phi}}{\tilde{\omega}} \left(1 + \delta^2 \left\{ \frac{1}{4} + \frac{\Delta_2}{\Delta} \tilde{\omega}^2 \right\} \right) \right], \quad (\text{S29})$$

$$\bar{\beta} = -\arcsin \left[\frac{c_{\bar{\theta}} \tilde{\omega}}{p s_{\Phi}} \left(1 - \delta^2 \left\{ \frac{1}{4} + \frac{\Delta_3}{\Delta} p \tilde{\omega}^2 \right\} \right) \right], \quad (\text{S30})$$

$$(\text{S31})$$

with

$$\Delta = c_{\Phi}^4 (p-1)^2 - c_{\Phi}^2 \tilde{\omega}^2 (p-1)^2 + \tilde{\omega}^2 p^2, \quad (\text{S32})$$

$$\Delta_2 = (p-1) c_{\Phi}^2 - 2p^2 + \tilde{\omega}^2 (p^2 - p + 1), \quad (\text{S33})$$

and

$$\Delta_3 = p(p-1) c_{\Phi}^2 - p(p+1) + \tilde{\omega}^2. \quad (\text{S34})$$

In the particular case of the planar object with zero diagonal elements $\text{Ch}_2 = \text{Ch}_3 = 0$, the relations (S26) reduce to these in Eqs. (S12).

C. High-frequency wobbling regime

In the high-frequency wobbling regime the propulsion velocity is found in the following way. First, we use the Eqs. (S4)-(S6), (S18)-(S23) for the velocity components U_X , U_Y and U_Z in terms of three non-trivial chirality coefficients Ch_2 , Ch_3 and Ch_{13} . Then for the time derivatives $\dot{\varphi}$, $\dot{\psi}$ and $\dot{\theta}$ we use their explicit dynamic relations (5)-(7) in the main text. Retaining only the terms at zero frequency we finally obtain:

$$\begin{aligned} \bar{U}_X / \omega \ell = & \text{Ch}_3 s_{\bar{\theta}} s_{\bar{\varphi}} - \text{Ch}_2 \frac{1}{4b\tilde{\omega}} s_{2\alpha} s_{\Phi} s_{\bar{\theta}}^2 + \text{Ch}_{13} \frac{1}{(p+1)c_{\Phi}\tilde{\omega}} \left[\frac{2pc_{\Phi}^2(1+c_{\bar{\theta}})-s_{\Phi}^2}{4} b s_{2\bar{\varphi}} c_{\alpha} - \frac{p}{2b} s_{\bar{\theta}}^2 s_{\Phi}^2 s_{\alpha} - \right. \\ & \left. \frac{s_{\Phi}^2}{2b} \left(c_{\bar{\theta}} + \frac{2}{t_{\Phi}^2} - a^2 - b^2 - 1 + \frac{2a^2+b^2}{1+c_{\bar{\theta}}} \right) s_{\alpha} - \frac{p}{bc_{\bar{\theta}}^2} ((c_{\bar{\theta}}+1)^2 - a^2)(c_{\bar{\theta}} - s_{\Phi}^2)(c_{\bar{\theta}} - 1) s_{\alpha} \right], \quad (\text{S35}) \end{aligned}$$

$$\begin{aligned} \bar{U}_Y / \omega \ell = & -\text{Ch}_3 s_{\bar{\theta}} c_{\bar{\varphi}} - \text{Ch}_2 \frac{b}{4\tilde{\omega}} s_{\Phi} (c_{\bar{\theta}} c_{2\alpha} + \frac{1}{2} s_{\bar{\theta}}^2 s_{2\bar{\varphi}} s_{2\alpha}) + \text{Ch}_{13} \frac{p}{(p+1)c_{\Phi}\tilde{\omega}} \left(a s_{\bar{\theta}} c_{\bar{\varphi}} c_{\Phi}^2 - \frac{b}{2} s_{\Phi}^2 c_{\bar{\theta}} \right) c_{\alpha} - \\ & - \text{Ch}_{13} \frac{1}{4(p+1)c_{\Phi}\tilde{\omega}} \left[\{ p c_{\bar{\theta}}^2 (-3 + c_{\Phi}^2) + c_{\bar{\theta}} (2p c_{\Phi}^2 + s_{\Phi}^2) + 3p s_{\Phi}^2 - 2c_{\Phi}^2 \} b s_{2\bar{\varphi}} s_{\alpha} + , \right. \\ & \left. + \{ (a^2 + b^2) s_{\Phi}^2 c_{\bar{\theta}} - 2(a^2 + c_{\Phi}^2) + \frac{2a^2(1+c_{\Phi}^2)}{1+c_{\bar{\theta}}} \} \frac{2}{b} c_{\alpha} \right], \quad (\text{S36}) \end{aligned}$$

$$\begin{aligned} \bar{U}_Z / \omega \ell = & \text{Ch}_3 c_{\bar{\theta}} - \text{Ch}_2 \frac{b}{4\tilde{\omega}} s_{\Phi} s_{\bar{\theta}} (c_{\bar{\varphi}} c_{2\alpha} - s_{\bar{\varphi}} s_{\bar{\theta}} s_{2\alpha}) + \text{Ch}_{13} \frac{1}{(p+1)c_{\Phi}\tilde{\omega}} \left[\left(\frac{p}{2} s_{\Phi}^2 s_{\bar{\theta}}^2 - c_{\Phi}^2 \right) s_{\alpha-\bar{\xi}} - \right. \\ & \left. - a p c_{\Phi}^2 c_{\bar{\theta}} c_{\alpha} + \left\{ \frac{s_{\Phi}^2 s_{\bar{\theta}}^2}{c_{\bar{\theta}}} + (p+1) s_{\Phi}^2 - 1 - p c_{\bar{\theta}} (c_{\bar{\theta}} + c_{\Phi}) \right\} c_{\bar{\xi}} s_{\alpha} \right]. \quad (\text{S37}) \end{aligned}$$

IV. When the mutual interactions among propellers are negligible?

In this section we consider the effect of the mutual magnetic and hydrodynamic interactions on the micromotor dynamics and provide an estimate of their density in the swarm for which these effects can be neglected. The consideration is done under the following simplifying assumptions:

- a) the external rotating magnetic field is symmetric (i.e, \mathbf{H}_{rot}) with $\delta = 0$;
- b) we consider helical micromotors that propel without wobbling, i.e., with $\theta = 0$ such that the magnetic moments of all micromotors rotate in the plane of the field with its angular frequency ω ;
- c) the magnetic and hydrodynamic interactions are considered separately.

1. Magnetic interactions

Two magnetic nanomotors with permanent magnetic moment \mathbf{m}_1 and \mathbf{m}_2 interact with each other via dipolar-dipolar potential

$$\mathcal{U}_d = \frac{\mathbf{m}_1 \cdot \mathbf{m}_2}{r^3} - 3 \frac{(\mathbf{m}_1 \cdot \mathbf{r})(\mathbf{m}_2 \cdot \mathbf{r})}{r^5}, \quad (\text{S38})$$

Averaging Eq. (S38) over the period of the rotating field determines the mean value of the potential in the form

$$\bar{\mathcal{U}}_d = -\frac{m_1 m_2}{2r^3} [1 - 3(\mathbf{k} \cdot \mathbf{n})^2], \quad (\text{S39})$$

where \mathbf{k} is the unit vector along the Z -axis, \mathbf{n} is the interparticle vector and $\mathbf{n} = \mathbf{r}/r$.

The magnetic interaction affects the dynamics in two ways: (i) it modifies the value of the external rotating field \mathbf{H}_{rot} in the vicinity of, e.g., propeller #2 by the value $\mathbf{H}_{loc} = -\partial \bar{\mathcal{U}}_d / \partial \mathbf{m}_2$; (ii) nanopropellers in a ‘‘side-by-side’’ configuration attract each other and may form an aggregate in a finite time.

The following estimates of the magnitude of the mutual magnetic interaction rely on the data from Ref. [5] where the experiments on propulsion of a swarm of magnetic microhelices in the vitreous body of the eye were reported. The length of the microhelix was $\ell = 2 \mu\text{m}$ and its diameter $d = 500 \text{ nm}$. The magnetic moment of propellers is about $m \approx 1.5 \cdot 10^{-13} \text{ emu}$, the viscosity of the vitreous is $\eta = 1.4 \cdot 10^{-2} \text{ P}$, the amplitude of the rotating field is $H_{rot} = 25 \text{ Oe}$, the propulsion velocity is $U = 10.6 \mu\text{m/s}$ and the characteristic time required for the microhelices to reach the retina from the center of the vitreous is $t_{exp} = 30 \text{ min}$.

At the distance $r \approx 1 \mu\text{m}$, the local magnetic field $H_{loc} \sim m/r^3 \sim 0.1 \text{ Oe}$, which is two orders-of-magnitude lower than the external magnetic field H_{rot} , i.e., $H_{loc} \ll H_{rot}$. Thus, the distortion of the external magnetic field due to presence of a neighbor microhelix is negligible already at the separation distance equal to its length, ℓ .

Let us now consider magnetic attraction of two micromotors in the plane ($\mathbf{k} \perp \mathbf{n}$) of the field rotation. The balance of the magnetic and hydrodynamic forces reads

$$\zeta_{\perp} L \frac{dr}{dt} = -\frac{3}{2} \frac{m_1 m_2}{r^4}, \quad (\text{S40})$$

where $\zeta_{\perp} = 4\pi\eta/\ln(\ell/d)$ is the approximate transverse drag coefficient of the slender object [6]. Integration of Eq. (S40) yields the typical time t_{agg} it takes for two propellers initially separated by the distance r to aggregate. Over the time of the propulsion experiment, t_{exp} , the field induced aggregation is negligible when the mean separation distance between the propellers satisfy $r \gg r_* = [15m_1 m_2 t_{exp}/(2\zeta_{\perp} \ell)]^{1/5}$. Substituting the above values of m , t_{exp} , η , L , and d we find $r_* \approx 4 \mu\text{m}$.

Notice that the estimate is based on the implicit assumption that the propellers belong in the same XY -plane of the field rotation at all times. Actually, the propellers exhibit some variance of the propulsion speed related to non-uniformity of their geometry and magnetization. According to Ref. [7], that used the same microfabrication technique was as in [5], the standard deviation of the propulsion velocity $\sigma = 0.2\text{--}0.3$. Therefore, a weaker condition is required in order to avoid the magnetic aggregation by requiring that the transverse velocity due to the micropropellers' magnetic interaction in Eq. (S40) is smaller than their relative velocity along the Z -axis:

$$\frac{dr_{\perp}}{dt} < \sigma U. \quad (\text{S41})$$

In this way we obtain a new estimate for the limiting interparticle distance

$$r_{*,magn} = [3m_1 m_2 / (2\zeta_{\perp} \ell \sigma U)]^{1/4}. \quad (\text{S42})$$

Even for quite underestimated value of the dispersion, $\sigma = 0.05$, we obtain $r_{*,magn} \approx 0.7 \mu\text{m}$. Thus, the magnetically-driven aggregation is not operable if the mean interparticle distance exceeds $r_* \approx 1 \mu\text{m}$. Moreover, typically the propellers in the swarm are inherently scattered along the Z -axis and thus their mean magnetic interaction is weaker than predicted above for side-by-side configuration that implies the fastest aggregation dynamics.

2. Hydrodynamic interactions

The main contributions to the hydrodynamic interaction are the driven rotation and translation of the propellers. The rotation contributes the *rotlet* term (the anti-symmetric part of the force dipole, [6]) generating the fluid flow with velocity \mathbf{v} related to the driven rotation with the angular velocity $\boldsymbol{\omega}$, $\mathbf{v} \sim (R/r)^3 \boldsymbol{\omega} \times \mathbf{r}$, where R is the effective radius of the propeller. For a slender, (e.g., helical) propeller of diameter d and length ℓ in the tumbling regime $R^3 \approx \ell(d/2)^2$ and in the wobbling regime (with small θ) we have $R \approx d/2$. This flow \mathbf{v} , however, only contributes to the rotation of a pair of propellers in the field XY -plane and do not perturb their relative motion. As shown in Ref. [8] for the swarm of sixteen magnetic propellers, these rotations do not affect their net motion along the Z -axis. The hydrodynamic interactions of the propellers located in different transverse planes perpendicular to the Z -axis proved to be negligible upon time-averaging [8]. Therefore, below we neglect the leading-order rotlet contribution to the flow and focus on the sub-leading term originated due to propulsion.

Since the propulsion of a propeller in the rotating magnetic field is force-free, we assume that at some distance away from the propeller the flow \mathbf{v} is due to the symmetric part of the force dipole or the *stresslet* [6]:

$$\mathbf{v} = -\frac{p\mathbf{n}}{8\pi\eta r^2}[1 - 3(\mathbf{k} \cdot \mathbf{n})^2], \quad (\text{S43})$$

where the dipole strength, $p \sim \eta U \ell^2$ [9]. The effect of the hydrodynamics is similar to that of the magnetic interactions, while, the strength of the hydrodynamic interaction in (S43) decays slower ($\sim 1/r^2$) than the magnitude of the magnetic interaction in (S40) ($\sim 1/r^4$).

Similar to previous analysis, we estimate the role of the hydrodynamic interactions in two ways. First, we consider two propellers located in the XY -plane of the field and compare their propulsion velocity U with the magnitude of the advective flow v originated by the nearby propeller,

$$v/U = \frac{p}{8\pi U \eta r^2} \sim \frac{1}{8\pi} \left(\frac{\ell}{r}\right)^2. \quad (\text{S44})$$

The estimate implies that the dynamics of the propeller does not change dramatically if the reference propeller is separated by the distance $r \geq \ell$ from its neighbor.

Second, let us determine the typical distance $r_{*,hyd}$ at which the advective velocity v is

equal to the relative velocity σU of propellers moving along the Z -axis. For $r_{*,hyd}$ we find

$$r_{*,hyd} = \frac{\ell}{\sqrt{8\pi\sigma}}. \quad (\text{S45})$$

For the experimentally observed dispersion $\sigma = 0.2\text{--}0.3$ and $\ell = 2 \mu\text{m}$ we have $r_{*,hyd} \approx 0.9 \mu\text{m}$.

Combining the both considerations of magnetic and hydrodynamic interactions one can conclude that they can be safely neglected given that the mean inter-particle distance in the swarm satisfy $r \approx 2 \mu\text{m}$. This estimate corresponds to the average motor number density $n < n_* \sim 10^{17} \text{ m}^{-3}$.

-
- [1] L. D. Landau, E. M. Lifshitz, *Mechanics*, 3rd ed.; Pergamon Press, Oxford, 1976.
- [2] J. Diebel, *Representing Attitude: Euler Angles, Unit Quaternions, and Rotation Vectors*; Matrix, Citeseer, 2006.
- [3] R. S. Berman, O. Kenneth, J. Sznitman and A. M. Leshansky, *New J. Phys.*, 2013, **15**, 075022.
- [4] K. I. Morozov, Y. Mirzae, O. Kenneth, and A. M. Leshansky, *Phys. Rev. Fluids*, 2017, **2**, 044202.
- [5] Z. Wu, J. Troll, H.-H. Jeong, Q. Wei, M. Stang, F. Ziemssen, Z. Wang, M. Dong, S. Schnichels, T. Qiu, and P. Fischer, *Sci. Adv.*, 2018, **4**, eaat4388.
- [6] S. Kim and S. J. Karrila, *Microhydrodynamics*, Butterworth-Heinemann: Boston, 1991.
- [7] D. Walker, M. Kubler, K. I. Morozov, P. Fischer, and A. M. Leshansky, *Nano Lett.*, 2015, **15**, 4412–4416.
- [8] J. Buzhardt and P. Tallapragada, *Phys. Rev. E*, 2019, **100**, 033106.
- [9] The far-field flow induced by various *self-propelled* (force- and torque-free) swimmers can typically be well described by the stresslet in (S43). Apparently in the far-field flow due to *externally (torque-)driven* rigid *helix* there is no stresslet, and the sub-leading term (after rotlet) is due to *source doublet* (decaying like $1/r^3$). Therefore, the present analysis based on the stresslet may somewhat overestimate the effect of the hydrodynamic interactions. The detailed analysis of the flow around the torque-driven propeller will be conducted elsewhere.